JOURNAL OF Materials CHEMISTRY

The synthesis and characterisation of mixed Y_2O_3-doped ZrO_2 and α-Fe_2O_3 nanosized powders

Tomas Raming, Louis Winnubst* and Henk Verweij†

Laboratory for Inorganic Materials Science, Faculty of Chemical Technology and MESA$^+$ Research Institute, University of Twente, P.O. Box 217, 7500 AE Enschede, The Netherlands. E-mail: a.j.a.winnubst@ct.utwente.nl

Received 2nd July 2002, Accepted 2nd August 2002
First published as an Advance Article on the web 3rd October 2002

Several wet chemical precipitation methods used to synthesise nanocrystalline composite powders containing zirconium oxide, yttrium oxide and iron(III) oxide are described. The crystallisation and phase composition of the precipitates were studied as a function of temperature. A co-precipitation method was compared with two different sequential precipitation routes. The amount of iron(III) oxide added varied from 27 to 42 mol% $FeO_{1.5}$. The dried gel obtained after co-precipitation was extensively studied as a function of calcination temperature. After calcination for 2 hours at 600–700 °C about 10–16 mol% $FeO_{1.5}$ was dissolved in the zirconia matrix. A part of the ferric oxide was present outside of the zirconia lattice, either as a crystalline hematite phase (when adding >40 mol% $FeO_{1.5}$), or as a finely dispersed amorphous ferric oxide (when adding <34 mol% $FeO_{1.5}$). After calcination at temperatures around 900 °C only a few mol% $FeO_{1.5}$ were dissolved in the zirconia matrix. All sequential precipitation routes resulted in dual-phase yttria-doped zirconia and hematite powders after calcination. Only up to 4 mol% of ferric(III) oxide could be dissolved in the zirconia lattice when using a sequential precipitation route.

Introduction

Although there have been many reports on the synthesis and properties of zirconia–hematite powders,[1–5] densification of these powders into zirconia–hematite ceramics has rarely been reported.[6,7] Yet zirconia–hematite ceramics can have interesting properties, especially when the zirconia phase has a tetragonal or cubic structure, since both tetragonal and cubic zirconia are oxygen-ion conducting.[8] The tetragonal and cubic phase of zirconia, which normally has a monoclinic structure, are usually obtained by doping the zirconia with yttria. If the zirconia phase is doped with 3–6 mole% Y_2O_3, normally the tetragonal phase is obtained; if the amount of yttria dopant is higher the zirconia becomes cubic.[8]

Since the hematite phase is (semi)-electron conducting, zirconia–hematite materials can show mixed ionic–electronic conduction, depending on the proportions and distribution of the two phases and the amount of yttria doping in the zirconia phase.[6,7] Furthermore, it has been shown that tetragonal zirconia, unlike cubic zirconia, can be densified into a ceramic with grains that are a very small size, below 100 nm, which leads to properties deviating from those of ceramics with micron-sized grains.[9] The nanosize of the grains of a ceramic can open a whole new spectrum of properties. Hardly any research has been done yet into the synthesis and properties of dual-phase ceramics with nano-sized grains; mainly single-phase ceramics with nanosized grains have been obtained.[9]

The first step in obtaining nano-grained dual-phase zirconia–hematite ceramics with interesting properties is the synthesis of a powder mixture of tetragonal zirconia and hematite. Many options are available for making such a powder,[1–5] but the method of synthesis has to be considered well. If hematite–zirconia ceramics with grains <100 nm in size are to be obtained, it is a necessity that the crystallites of the starting powders have nano-dimensions as well, since the crystallites grow in size during the sintering process. It is also important that the two phases are homogeneously distributed, since this will increase the mutual hindrance between the two phases. The mutual hindrance will reduce the coagulation of grains during the sintering process, as is known from zirconia–alumina composites, which will keep the grains small.[10] Simple powder mixing of two separately prepared powders (a zirconia and hematite powder) with nanosized crystallites might seem the easiest solution, but it is unlikely that this will lead to a homogeneous distribution of the zirconia and hematite crystallites. The smaller the crystallites, the stronger the aggregates they form. Therefore, it is preferable to prepare the two phases *in situ*, instead of mixing two separately prepared powders.

This publication discusses different methods of powder synthesis that have been used to make crystalline hematite–zirconia powders with particles of nano-dimensions. A co-precipitation technique is compared with different sequential precipitation techniques in order to probe the influence of the synthesis technique on the crystallite size, phase composition and distribution of the phases of the resulting powders.

The aspect that is investigated here most thoroughly is the solid solubility of Fe^{3+} ions in the zirconia phase. Many communications have reported on the solid solubility of Fe^{3+} in zirconia, all mentioning different solubility limits even when using seemingly identical methods of synthesis.[3,11] The vast majority of the zirconia–hematite mixed powder reports describe the use of undoped zirconia,[12–15] however, some reports on the synthesis of mixed yttria-doped zirconia–hematite powders also exist.[16–18] It is not really known though, what influence the presence of yttria has on the solid solubility of Fe^{3+} in zirconia.

A solid solution of hematite in zirconia will by definition have a more homogeneous distribution of the two elements Fe and Zr (you cannot speak about distribution of two phases, in this case) than a two-phase zirconia–hematite mixture. Here it is investigated how a solid solution can be obtained, and how stable this solid solution is, in order to be able to tune the distribution of the hematite and zirconia while maintaining a small crystallite size, thereby obtaining powders that are fit to be densified into hematite–zirconia ceramics with grains <100 nm in size.

†Present address: Department of Materials Science and Engineering, The Ohio State University, Columbus, OH 43210-1178, USA.

Experimental

Two general synthesis routes have been used to make the powders: co-precipitation and sequential precipitation. When performing a sequential precipitation either the hematite or zirconia phase was made first.

For the CP (co-precipitation) method, an aqueous solution was prepared from $ZrOCl_2 \cdot 8H_2O$ (Merck), YCl_3 (Cerac) and $FeCl_3 \cdot 6H_2O$ (Fluka). The total molar amount of $ZrOCl_2 \cdot 8H_2O$ was 0.15 mol l^{-1} for all solutions, while the concentration of $FeCl_3 \cdot 6H_2O$ was varied from 0.06 to 0.11 mol l^{-1}. The ratio Zr^{4+} : Y^{3+} was maintained at a 95 : 5 mol ratio for each synthesis. The solution (pH $\sim$ 1.5) was filtered over a 0.025 μm membrane to remove any insoluble species, after which it was slowly added to an excess of concentrated aqueous ammonia (pH $\sim$ 14) solution over a 4–6 hour period. The ammonia solution was stirred vigorously and continuously with a top-mounted turbine stirrer. The metal-ion containing solution was added with the aid of a peristaltic pump through a tube with an opening of 1.5 mm diameter. The end of the tube was placed directly above the tip of the stirrer to maximise the number of nucleation sites (and minimise nucleus growth). The resulting gel was filtered and washed with distilled water to remove the chloride ions until the pH had decreased to 9. The precipitate was finally washed with ethanol until the density of the filtrate was below 0.79 g cm^{-3} (*i.e.* water content $<5\%$). The gel, suspended in ethanol, was then oven-dried overnight at 100 °C. The resulting amorphous powder was ground in a mortar and then calcined in air at different temperatures for 2 hours at a heating rate of 2 °C min^{-1}.

When using the SPZH-method (sequential precipitation: first zirconia then hematite) a zirconia suspension was first prepared by hydrothermal crystallisation of a solution of $ZrOCl_2 \cdot 8H_2O$ (Merck) and YCl_3 (Cerac) for 2 hours at 200 °C,[19] after which ferric hydroxide was precipitated within this suspension by adding a $FeCl_3 \cdot 6H_2O$ solution and subsequently raising the pH. The hydrothermal crystallisation step resulted in an aqueous basic suspension of nanosized (average grain size 8 nm) crystalline 3Y-TZP (tetragonal zirconia doped with 3 mol% of Y_2O_3).[19] The zirconia suspension was added to the aforementioned mixing and reaction set-up. $FeCl_3 \cdot 6H_2O$ solutions in varying concentrations were added while vigorously stirring, leading to an acidic suspension. The pH of the suspension was increased from 1–2 to 6–7 by the slow and homogeneous addition of ammonia while vigorously stirring, inducing the precipitation of ferric hydroxide species in the zirconia gel. The resulting mixed gel was washed, dried and calcined as described above.

For the SPHZ-method (sequential precipitation: first hematite then zirconia) nearly spherical crystalline hematite particles were first made by heating a 0.02 M $FeCl_3 \cdot 6H_2O$ solution at 100 °C in a closed vessel for 24 hours.[11] The pH during precipitation was 1.5 to 2. The acidic hematite suspension was mixed with an equal volume of aqueous ammonia (pH = 14) in the mixing–precipitation vessel, which resulted in a pH of 11. A solution of $ZrOCl_2 \cdot 8H_2O$ and YCl_3 was slowly added to this suspension. The resulting gel was washed to remove the chloride. The water in the gel was replaced by ethanol, after which the gel was dried at 100 °C and calcined in air at 525 °C. The resulting powder contained 34 mol% $FeO_{1.5}$.

For the second SPHZ-synthesis the hematite preparation was identical, but the zirconia precipitation deviated. The acidic hematite suspension was added to the mixing–precipitation set-up and heated to 90 °C. To this hot suspension aqueous solutions of $ZrOCl_2 \cdot 8H_2O$ plus YCl_3 and urea were added. The following reaction took place:

$$O{=}C(NH_2)_2 + 3H_2O \rightarrow CO_2\,(g) + 2NH_4OH$$

Due to the *in situ* production of ammonia the pH was increased to 6–7, inducing the precipitation of the zirconia and yttria hydroxides. The resulting gel was subsequently washed with water and ethanol. The gel was dried in a furnace at 100 °C, ground in a mortar and calcined at 600 °C. The resulting powder contained 43 mol% $FeO_{1.5}$.

The elemental composition was determined by X-ray fluorescence (XRF). About 400 mg of the powders were mixed with 5600 mg $Li_2B_4O_7$ in a mortar. This mixture was heated to 1100 °C to form a liquid that was poured into a Pt casting dish to form a fused bead. The loss of ignition was determined by measuring a blank with only $Li_2B_4O_7$. The elemental composition of the bulk powders was determined with a Philips PW 1480/10-fluorometer. Every measurement was done in duplicate. The software program X-40 (Philips) was used to calculate the calibration curve. α-Factors were used to correct for matrix effects.

For powder X-ray diffraction (XRD) and X-ray line broadening (XRLB) measurements two types of diffractometers were utilised. Data for the phase composition of the calcined powders were collected at room temperature on a Philips X′Pert-1 PW3710 diffractometer using Cu-Kα (λ = 1.542 Å) radiation and a Ni-filter. The same apparatus was used to measure the X-ray line broadening (XRLB) to determine the average crystallite size of the phases of the powders by the Scherrer formula.[20]

The amorphous-to-crystalline transitions were monitored from variable temperature XRD data obtained on a Philips X′Pert MPD HTK-16 (Anton Paar) diffractometer equiped with a Cu-tube, a secondary curved graphite monochromator and an automatic divergence slit. A few milligrams of non-calcined powder were dispersed onto a Pt-foil. The foil was heated in a high temperature XRD (HT-XRD) chamber to 1000 °C at a rate of 2 °C min^{-1}. The temperature was raised with 100 °C increments and kept constant for 2 hours at each temperature after which the XRD spectrum of the powder was measured *in situ*. Following the measurement at 1000 °C, the powder was cooled to room temperature where another XRD measurement was performed.

The crystallisation behaviour of the dried gels was also analysed by differential scanning calorimetry (DSC). Approximately 50 mg of each non-calcined powder was heated to 1000 °C with 10 °C min^{-1} in an alumina crucible in air using a Setsys-18 thermal analyser with a DSC-1500 measuring head (Setaram). Upon reaching the highest programmed temperature, the powders were cooled down immediately. The phase composition of the powders after the DSC measurements was verified by XRD.

Transmission electron microscopy (TEM) coupled with energy dispersive X-ray analysis (EDX) was performed with a Philips EM30 Twin/STEM TEM, provided with a KEVEX Delta-Plus EDX to determine the crystallite size and the chemical composition. The spot diameter for EDX measurement in all cases was 34 nm. The samples were prepared by addition of alcohol and dispersion by ultrasonification for 10 minutes. One drop of the suspension was added to a copper grid that was air-dried prior to use.

Results

The elemental compositions of the calcined powders were determined with XRF and are shown in Table 1. The calcination temperatures of the different powders are also given in Table 1. The calcination temperatures that were used were the minimal temperatures necessary to obtain fully crystalline oxide phases for each powder.

To determine the temperatures, at which the phases of the different precipitated powders crystallised, the precipitates were investigated with high-temperature XRD and DSC. It should be noted that the temperature in the XRD measurement

Table 1 Quantitative XRF data showing the molar composition of the calcined powders and the calcination temperatures (with 2 hours of calcining)

Powder	Calcination Temperature/°C	ZrO_2 (mol%)	$FeO_{1.5}$ (mol%)	$YO_{1.5}$ (mol%)	HfO_2 (mol%)
CP42	600	54.5	42.0	3.0	0.6
CP40	600	56.6	39.8	2.9	0.6
CP34	700	62.4	33.6	3.3	0.7
CP27	700	68.5	26.9	3.8	0.8
SPZH42	600	55.1	41.9	3.0	0.0
SPZH34	500	63.1	33.7	2.5	0.7
SPZH27	500	69.1	27.0	3.8	0.0
SPHZ43	600	53.6	43.8	2.7	0.0
SPHZ34	525	63.3	34.1	2.6	0.0

Table 2 Phase formation temperatures (in °C) according to HT-XRD and DSC measurements

Powder	Zirconia		Hematite	
	HT-XRD	DSC	HT-XRD	DSC
Fe_2O_3			200–300	384
SPZH34	[a]	[a]	400–500	454
SPZH42	[a]	[a]	400–500	475
SPHZ43	400–600	511	[a]	[a]
SPHZ34	400–500	488	[a]	[a]
3Y-TZP	400–500	440		
CP42	400–600	668	400–600	668
CP40	400–600	659	400–600	659
CP34	500–700	673	700–800	842
CP27	500–700	659	800–900	875

[a]These crystal phases were already present at the start of the measurements.

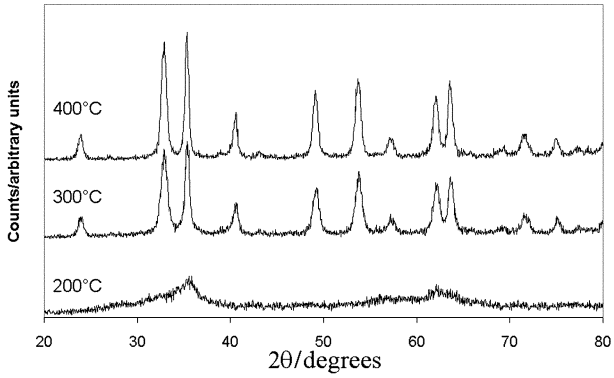

Fig. 1 High temperature XRD patterns of precipitated hydrated ferric oxide powder after drying at 100 °C.

chamber was raised at 2 °C min^{-1} (and held for 2 hours after each 100 °C increment), while the DSC-measurements were performed at a continuous heating rate of 10 °C min^{-1}.

Crystallisation temperatures are given in in Table 2. The hydrated ferric oxide powder was prepared by precipitation, in the same manner as the hydrated ferric oxide of the SPZH powders, but of course in the absence of zirconia particles. The HT-XRD of the hydrated ferric oxide is shown in Fig. 1. An amorphous zirconia oxyhydroxide powder, doped with 5.8 mol% $YO_{1.5}$ (3Y-TZP), was prepared for comparison as well. This powder was precipitated using the co-precipitation technique. The HT-XRD of the amorphous zirconia oxyhydroxide powder can be seen in Fig. 2.

Table 2 shows that the hydrated ferric oxide powder crystallised between 200 and 400 °C to form hematite (α-Fe_2O_3) if no zirconia was present. If zirconia crystallites were present in a mix with hydrated ferric oxide, as was the case with the

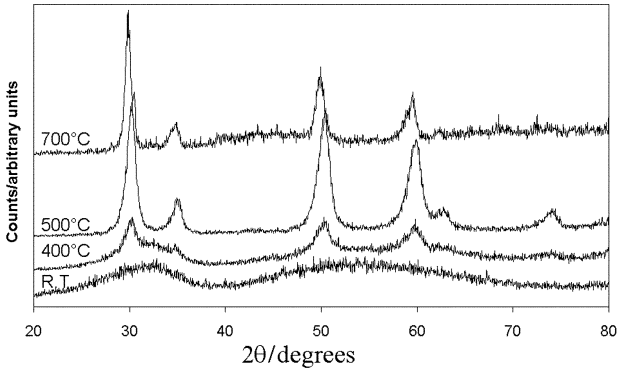

Fig. 2 High temperature XRD patterns of precipitated 3Y-TZP powder after drying at 100 °C.

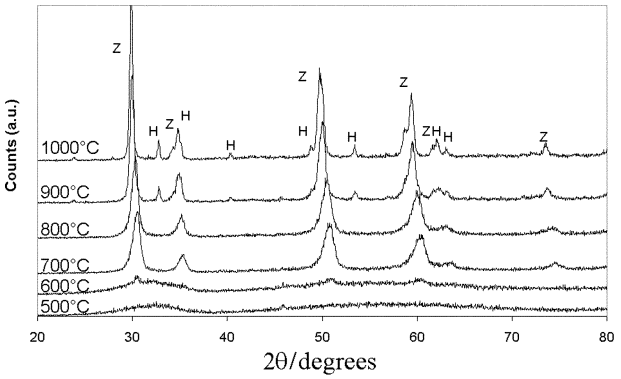

Fig. 3 High temperature XRD patterns of the non-calcined CP27 powder after drying at 100 °C. Z = ZrO_2, H = Hematite (α-Fe_2O_3).

non-calcined SPZH42 and SPZH34 powders, the hydrated ferric oxide crystallised at higher temperatures (between 400 and 500 °C). The presence of the zirconia crystallites seems to have inhibited the crystallisation of the hematite phase. In the case of the SPHZ powders the crystallisation of the amorphous zirconia phase was also inhibited when it was precipitated in a suspension of crystalline (hematite) particles, from comparison of the higher crystallisation temperature of the zirconia phase of the SPHZ powders with that of the 3Y-TZP powder.

The crystallisation behaviour of the co-precipitated powders was quite different compared to that of the sequentially precipitated powders. Fig. 3 shows the HT-XRD patterns of non-calcined CP27 powder. Crystallisation of the zirconia phase started at around 600 °C, 200 °C higher than the single phase 3 mol% yttria-doped zirconia. XRD peaks of the hematite phase became visible only at 900 °C. For the CP34 powder crystallisation of the zirconia phase also started at around 600 °C, but peaks of the hematite phase were present at 800 °C, as can be seen in Fig. 4. After cooling to room temperature, the XRD was identical to the XRD at 1000 °C, for all measured powders.

The zirconia and hematite phase of the non-calcined CP40 powder started to form respectively at <500 °C and between 500 and 600 °C as shown in Fig. 5. The non-calcined CP42 powder showed the same HT-XRD patterns as the CP40 powder. The DSC-diagrams of the four non-calcined CP powders are shown in Fig. 6. All CP powders showed a strong and short exothermic reaction with an onset-temperature of 659–673 °C. It is likely that the exotherms between 600 and 700 °C, visible in the DSC diagrams of the CP40 and CP42 powders, indicate simultaneous crystallisation of the majority phase, zirconia, and the minority phase, hematite, since there were no other exotherms above 400 °C.

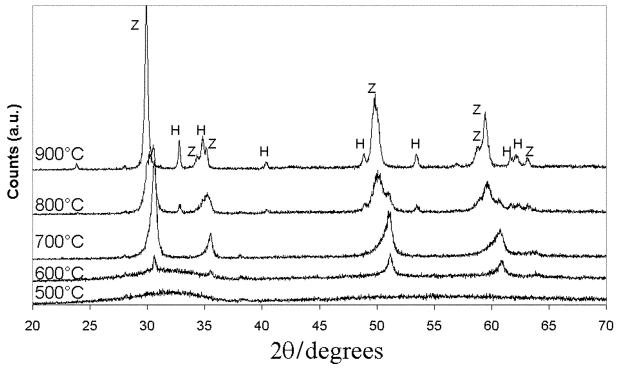

Fig. 4 High temperature XRD patterns of the non-calcined CP34 powder after drying at 100 °C. Z = ZrO_2, H = Hematite (α-Fe_2O_3).

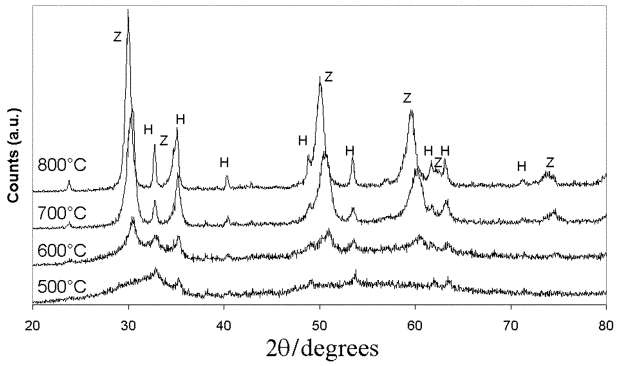

Fig. 5 High temperature XRD patterns of the non-calcined CP40 powder after drying at 100 °C. Z = ZrO_2, H = Hematite (α-Fe_2O_3).

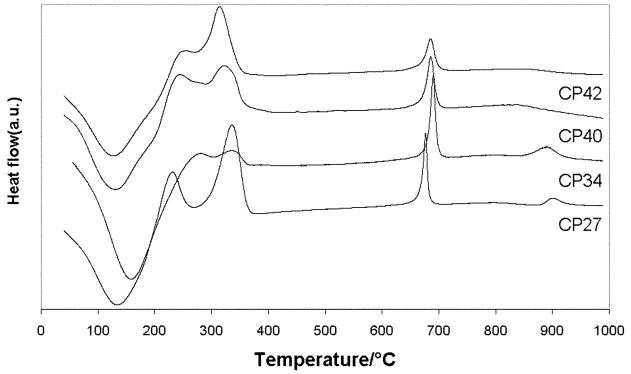

Fig. 6 DSC diagrams of the non-calcined CP powders (heating rate 10 °C min^{-1}).

The CP27 and CP34 powders both showed a second exothermic reaction with onset-temperatures of 875 and 842 °C, respectively. Since the HT-XRD measurements showed that the hematite phase occurred for both powders at these high temperatures, these exotherms may indicate the onset of the crystallisation of the hematite phase.

Due to the broadness of the XRD-signals, it was difficult to distinguish between tetragonal and cubic zirconia, but it is clear that no monoclinic zirconia is present in any of the calcined powders.

The 2θ value of the zirconia (111) reflection as a function of temperature was determined by HT-XRD for all non-calcined zirconia–hematite powders. The positions of the peaks were corrected using the Pt of the strip as reference. The zirconia

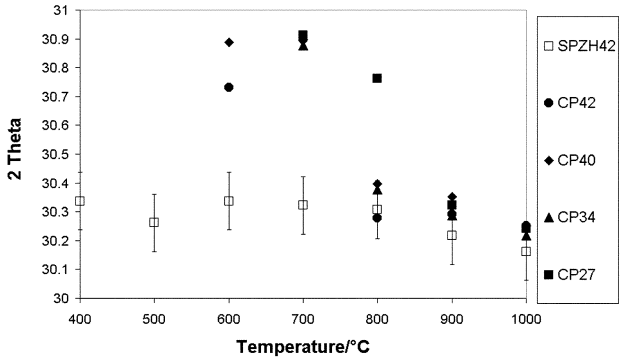

Fig. 7 Change in position of the zirconia (111) reflection of precipitated zirconia–hematite powders due to heating as measured by HT-XRD.

(111) 2θ values for all CP powders and the SPZH42 powder are shown in Fig. 7 as a function of temperature. The 2θ value of the zirconia (111) reflection did not change much with temperature for any of the SP powders, and in all cases was about 30.3° 2θ. Therefore, only the SPZH42 powder is shown in Fig. 7. The 2θ value of the zirconia (111) reflection was at around 30.8° 2θ for all CP powders up to 700 °C, both after 2 and 20 hours of calcination. A change in the peak position of the (111) reflection occurred between 700 °C and 800 °C in the case of the CP34, CP40 and CP42 powders. For CP27 this sudden decrease in 2θ-value, and thus increase in lattice constant, occurred between 800 °C and 900 °C. After this change the position of the zirconia (111) reflection of the CP powders was almost equal to the position of the zirconia (111) reflection of the SP powders.

The CP27 and CP34 powders were also calcined for a period of 20 hours at 700 °C, to check if a hematite phase would evolve. The CP34 powder indeed showed a small hematite peak after the 20 hours of calcination at 700 °C. The CP27 powder, however, did not show any hematite peak, even after 20 hours of calcination at 700 °C.

Several calcined zirconia–hematite powders were treated with boiling concentrated hydrochloric acid for several hours, to dissolve any amorphous or crystalline hematite present in the powders. Zirconia, whether it is monoclinic, tetragonal or cubic, does not dissolve in hydrochloric acid. The elemental compositions of the hydrochloric acid treated calcined powders were determined by XRF and are shown in Table 3.

Only for the SPHZ powders was it possible to clearly distinguish the hematite and zirconia crystallites when using TEM in combination with EDX. The SPHZ34 (calcined at 500 °C) and SPHZ43 (calcined at 600 °C) powders looked similar with TEM. No difference was observed in the microstructure properties between SPHZ powders prepared by the urea method (SPHZ43) or by means of direct precipitation (SPHZ34). Hematite crystallites of 40–70 nm were distributed throughout the clusters of zirconia crystallites of 5–10 nm, as can be seen in Fig. 8. The hematite crystallites were not distributed totally

Table 3 Quantitative XRF data showing the molar composition of the HCl-treated powders and the calcination temperature (after calcining for 2 hours)

Powder	Calcination Temperature/°C	ZrO_2 (mol%)	$FeO_{1.5}$ (mol%)	$YO_{1.5}$ (mol%)	HfO_2 (mol%)
CP42	600	85.6	9.5	4.1	0.9
CP40	600	83.0	11.8	4.3	0.8
CP34	700	79.0	16.2	4.1	0.8
CP34	900	92.1	2.8	4.3	0.9
CP27	700	84.6	11.1	3.4	0.9
SPZH34	500	91.7	3.8	3.5	1.0
SPHZ34	525	94.6	1.3	4.1	0.0

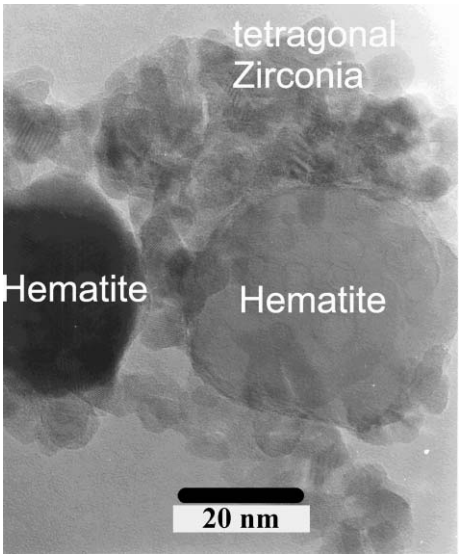

Fig. 8 TEM micrograph of the SPHZ43 powder after calcination at 600 °C for 2 hours.

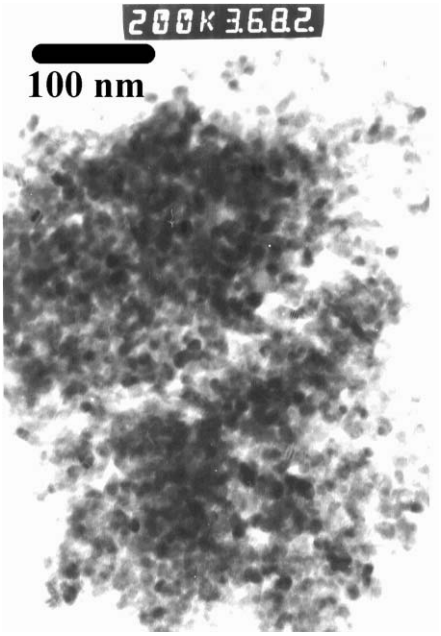

Fig. 9 TEM micrograph of the CP34 powder after calcination at 700 °C for 2 hours.

homogeneously through the powder; often they were present in clusters of up to ten crystals. However, for the SPZH and CP powders in general it was not possible to detect individual zirconia or hematite (if any present) crystals with TEM/EDX. Fig. 9 shows a TEM micrograph of the CP34 powder (calcined for 2 hours at 700 °C). No crystallites larger than 20 nm are discernible. The SPZH powders and the CP27 powder (calcined for 2 hours at 700 °C) looked similar to the TEM of the CP34 powder.

These TEM results were confirmed by X-ray line broadening measurements used to determine the average crystallite sizes of the phases present. The average crystallite sizes of the zirconia phases were almost identical for all powders; they varied from 7 to 8 nm. The crystallite sizes of the hematite phases varied more. The hematite crystals of the SPZH powders were the smallest, between 18 and 29 nm, while the SPHZ powders contained the largest hematite crystals, 70 nm for the SPHZ34 powder and 45 nm for the SPHZ43 powder. The two CP powders containing the crystalline hematite phase showed intermediate crystallite sizes for this hematite phase, 24 nm for the CP40 powder and 41 nm for the CP42 powder.

Discussion

Different methods have been used in this research to probe the composition and microstructure development of the synthesised zirconia–hematite powders. The combination of DSC and HT-XRD gives information on the crystallisation behaviour of the precipitated powders. In particular the crystallisation behaviour of the CP powders is remarkable.

In the literature, the absence of hematite XRD reflections combined with the presence of zirconia reflections has often been taken as evidence for the complete solvatin of the ferric oxide in the zirconia lattice.[11–13,17] Treatment of the co-precipitated powders hydrochloric acid (see Table 3) shows that this assumption cannot be made, making many of the reported claims on the solid solubility of ferric oxide in zirconia doubtful. Treatment with hydrochloric acid reveals the true amount of ferric oxide dissolved in the zirconia lattice. All non-dissolved iron oxide, whether crystalline or amorphous, dissolves in boiling hydrochloric acid. Only iron oxide present within the insoluble zirconia crystals can withstand this treatment. Therefore, it can be assumed that all iron oxide that is detected after this hydrochloric acid treatment was present within the zirconia crystallites.

The hydrochloric test shows that for not one of the CP powders did all the ferric ions added during precipitation dissolve in the zirconia phase. After co-precipitation the resulting gel consisted of an amorphous zirconium hydroxide network where the Zr^{4+} ions were connected by hydroxo bridges, as can de deduced from the two broad XRD signals in Fig. 3 centred around 35° 2θ and 60° 2θ respectively. In such an amorphous network the Zr^{4+} ions can readily be substituted by large amounts of Y^{3+} and Fe^{3+} ions.[21]

The crystallisation temperatures for both the zirconia and hematite phases of both the SP and CP powders are greater than those of the single-phase powders (see Table 2). The increases in the crystallisation temperatures of the zirconia phases of the SPHZ powders and the increases in the crystallisation temperatures of the hematite phases of the SPZH powders are only small compared to the increases in the crystallisation temperatures of both phases of the CP powders, especially when judging from the DSC data. The increase in the crystallisation temperature of the zirconia phase of the SPHZ powders and the hematite phase of the SPZH powders is mostly due to the hindering effect of the presence of the particles of the other phase, since the amount of solvation of the ferric oxide in the zirconia seems to be too low to account for this effect. The larger increase in crystallisation temperatures for the CP powders is indicative of a more homogeneous distribution of the two phases. This is for a large part caused by the fact that a substantial amount of ferric oxide is dissolved into the zirconia lattices of all CP powders after calcinations at $T \leqslant 700$ °C (see Table 3). An amorphous Zr–Fe–Y hydroxide network is formed upon precipitation. The presence of the ferric ions within this network obstructs the formation of the zirconia crystal phase, because at least a part of the ferric ions has to segregate out of this amorphous network, before crystallisation can occur.

It seems as if a meta-stable ZrYFe oxide phase is formed after calcination of the CP powders at temperatures of 600–700 °C. In this zirconia lattice about 10–16 mol% $FeO_{1.5}$ was dissolved. Upon further heating up to 900 °C only a few percent (<3 mol%) of the ferric oxide remained dissolved in the zirconia matrix (Table 3). This change in the amount of dissolved Fe ions in the zirconia lattice corresponds to the decrease in the 2θ value of the zirconia (111) reflections, as shown in Fig. 7, from 30.8° 2θ to a significantly lower value of

30.3° 2θ. The higher value for 2θ of the zirconia (111) reflection of the CP powders indicates that ferric ions have been dissolved in the zirconia lattice, substituting for Zr ions. Since ferric ions have a smaller ionic radius compared to zirconium ions, solvation of ferric ions in a zirconia lattice, by substitution for the zirconium metal ions, will therefore cause lattice contraction.[22] The amount of dissolved iron oxide left in the CP34 powder that was calcined at 900 °C is comparable to the amount of dissolved iron oxide in the calcined SP powders.

In the case of the CP27 and CP34 powders calcined at 700 °C for 2 hours formation of a hematite phase was not observed, even though segregation must also have occurred, since less than half of all ferric ions had dissolved in the zirconia lattice (compare Table 3 with Table 1). Even after calcining for 20 hours at 700 °C the CP27 powder does not show any evidence of a crystalline hematite phase. The question therefore is: in what form is the rest of the ferric oxide present?

Tabora and Davis[23] showed by using EXAFS that nanoclusters with Fe_2O_3 were present at the surfaces and defects of zirconia grains in zirconia doped with 2.3 mol% Fe_2O_3. No hematite phase was detected by XRD in this material. It might be that some ferric oxide is dispersed as nanoclusters in the CP powders, but is too small to be detected by XRD. The XRLB measurements and the TEM picture of CP34 (Fig. 9) show that the zirconia crystallites are extremely small, in between 5 and 10 nm. This small size provides a very large surface area, on which a large amount of ferric oxide nanoclusters could be dispersed.

XRD shows that for all the zirconia–hematite powders that are calcined at 900 °C or higher, the zirconia phase is tetragonal. At this temperature the ferric ions are largely segregated from the zirconia lattice (see for instance Table 3, the CP34 powder calcined at 900 °C). The fact that the zirconia remains tetragonal instead of becoming monoclinic demonstrates that the presence of yttria ensures that, when calcining these zirconia–hematite powders at a temperature of 900 °C or higher, the zirconia has the desired tetragonal structure. As can be seen in Table 3, the amount of yttrium ions dissolved in the zirconia lattice is independent of the amount of ferric ions present within the zirconia lattice. The yttrium ions, unlike the ferric ions, do not segregate from the zirconia lattice at higher calcination temperatures.

Furthermore, there is no indication that the presence of the yttrium ions influences the behaviour of the ferric ions. The effects for yttria-doped zirconia that is co-doped with ferric ions reported here are similar to the effects for zirconia doped solely with ferric ions. The ferric ions can be dissolved in comparable amounts, and they also segregate out of the zirconia lattice with increasing calcination temperature.[12,14,11]

The yttria-doped zirconia–hematite powders described here all show a small crystallite size of 7–8 nm for the zirconia crystallites. The size of the hematite crystallites, when present, however differs hugely. The SPHZ powders have hematite crystallites of 40–70 nm, which seems to disqualify these powders from being used to make zirconia–hematite ceramics with grains <100 nm in size. The SPZH powders have smaller hematite crystallites of 18–29 nm, which makes these powders more suitable for making nano-ceramics, and also because TEM did not show any clustering of the hematite crystallites. The CP powders, however, can be expected to have the most homogeneous distribution of zirconia and ferric ions, since a large number of the ferric ions were dissolved in the zirconia lattice. It might be advantageous to start densification with a largely single-phase CP powder, rather than an SPZH powder, in which the two phases are fully separated. The excretion of hematite out of the zirconia grains during sintering might have a severe retarding effect on grain growth. The CP powders with a lower percentage of hematite (CP27 and CP34) seem most suitable, since the CP42 powder has hematite crystallites of 45 nm.

Conclusions

Co-precipitation of an aqueous solution of zirconium, yttrium and ferric chloride salts by adding this solution to ammonia results in a homogeneous amorphous Zr–Y–Fe hydroxide network. The crystallisation of the zirconia phase out of this amorphous network occurred between 500 and 700 °C, which is significantly higher than single-phase 3Y-TZP, which crystallises between 400 and 500 °C. The crystalline zirconia phase that was formed upon calcination of the co-precipitated powders at 600 to 700 °C (2 hours) was a solid solution of 10 to 16 mol% of $FeO_{1.5}$ in $Zr_{0.95}Y_{0.05}O_{1.98}$. It has been shown here, that ferric oxide can remain amorphous up to a temperature of 800 °C, when it is finely dispersed between the nanosized zirconia crystals. When heating to 900 °C the large majority of the dissolved ferric ions were expelled from the zirconia lattice of the co-precipitated powders leaving less than 4 mol% $FeO_{1.5}$ in the zirconia matrix. When adding 40 or 42 mol% of ferric oxide, both the zirconia and hematite phases crystallised at around 500 °C, due to the large excess of ferric ions. When using a sequential precipitation technique, only a small amount (up to 4 mol%) of ferric oxide was dissolved in the zirconia lattice. The presence of yttrium ions in the zirconia does not influence the behaviour of the ferric ions, or *vice versa*.

First preparing a suspension of fine zirconia particles, and then precipitating ferric oxide particles into this suspension leads, after calcination, to a homogeneous distribution of fine zirconia (7–8 nm) and hematite (19–28 nm) crystallites. This powder seems suitable for use in making zirconia–hematite ceramics with grains <100 nm in size. The powders prepared by co-precipitation with a hematite percentage of 34 mole% or lower seem most suitable for this goal though, since they have the greatest homogeneous distribution of zirconia and ferric ions due to the large amount of solvation of ferric ions in the zirconia lattice.

Acknowledgements

Daphne Beukers and Jason Vu are gratefully thanked for the synthesis of zirconia–hematite powders. Mark Smithers is acknowledged for the EDX and TEM measurements and Herman Koster for the XRD and XRLB determinations. We are indebted to Werner van Zyl and Monserrat Garcia-Curiel for treatment of the zirconia–hematite powders with hydrochloric acid.

References

1 Z. Liu, Q. Dong and Y. Chen, *Mater. Chem. Phys.*, 1998, **53**, 67.
2 F. J. Berry, S. Jobsen and M. R. Smith, *Hyperfine Inter.*, 1989, **46**, 607.
3 K. Chen, Y. Fan, Z. Hu and Q. Yan, *Catal. Lett.*, 1996, **36**, 139.
4 V. R. Choudhary, B. S. Uphade, S. G. Pataskar and A. Heshavaraja, *Angew. Chem., Int. Ed. Engl.*, 1996, **35**, 2393.
5 J.-C. Wu, D.-S. Liu and A.-N. Ko, *Catal. Lett.*, 1993, **20**, 191.
6 G. A. Gogotski, *Ceram. Int.*, 1998, **24**, 589.
7 A. D. Neuimin, A. G. Kotlyar, S. F. Pal'guev, V. N. Strekalovskii and N. A. Batrakov, in *Electrochemistry of Molten and Solid Electrolytes*, Thermodynamics of Salt and Oxide Systems vol. 9, ed. S. F. Pal'guev, New York, 1972, p. 73.
8 S.-M. Ho, *Mater. Sci. Eng.*, 1982, **54**, 23.
9 P. Mondal, A. Klein, W. Jaegermann and H. Hahn, *Solid State Ionics*, 1999, **8**, 331.
10 A. Sturm, U. Betz, G. Scipione and H. Hahn, *Nanostruct. Mater.*, 1999, **11**, 651.
11 F. J. Berry, M. H. Loretto and M. R. Smith, *J. Solid State Chem.*, 1989, **83**, 91.
12 G. Štefanić, S. Musić, S. Popović and K. Nomura, *J. Mol. Struct.*, 1999, **480**, 627.
13 I. B. Inwang, F. Chyad and I. J. McColm, *J. Mater. Chem.*, 1995, **5**, 1209.
14 G. Štefanić, B. Gržeta and S. Musić, *Mater. Chem. Phys.*, 2000, **65**, 216.

15 S. Popovíc, B. Gržeta, G. Štefaníc, I. Czakó-Nagy and S. Musíc, *J. Alloys Compd.*, 1996, **241**, 10.
16 O. G. Ellert, I. A. Petrunenko, M. V. Tsodikov, O. V. Bukhtenko, D. I. Kochubey, Yu. V. Maksimov and A. Dominguez-Rodriguez, *J. Mater. Chem.*, 1996, **6**, 201.
17 Yu. N. Karavaev, Z. S. Martem'yanova and V. G. Zyryanov, *Inorg. Mater.*, 1995, **31**, 861.
18 O. G. Ellert, I. A. Petrunenko, M. V. Tsodikov, O. V. Bukhtenko, D. I. Kochubey, Yu. V. Maksimov, A. Dominguez-Rodriguez, F. L. Cumbreras and J. A. Navio, *J. Sol-Gel Sci.*, 1997, **8**, 213.
19 C. D. Sagel-Ransijn, A. J. A. Winnubst, A. J. Burggraaf and H. Verweij, *J. Eur. Ceram. Soc.*, 1996, **16**, 759.
20 P. Scherrer, *Goett. Nachr.*, 1918, **2**, 98.
21 G. T. Mamott, P. Barnes, S. E. Tarling, S. L. Jones and C. J. Norman, *J. Mater. Chem.*, 1991, **26**, 4054.
22 M. J. Verkerk, A. J. A. Winnubst and A. J. Burggraaf, *J. Mater. Sci.*, 1982, **17**, 3113.
23 J. E. Tabora and R. J. Davis, *J. Chem. Soc., Faraday Trans.*, 1995, **91**, 1825.